To appear in the *International Journal of Computational Fluid Dynamics*
Vol. 00, No. 00, 00 Month 20XX, 1–20

A coupled WC-TL SPH method for simulation of hydroelastic problems

Jiandong He[a,b], Nima Tofighi[b,*], Mehmet Yildiz[c], Juanmian Lei[a] and Afzal Suleman[b]

[a]*School of Aerospace, Beijing Institute of Technology, Beijing 100081, China*; [b]*Department of Mechanical Engineering, University of Victoria, Victoria, BC V8W 2Y2, Canada*; [c]*Integrated Advanced Manufacturing Technologies Research and Application Center, Faculty of Engineering and Natural Sciences, Sabanci University, Orhanli, Tuzla, 34956 Istanbul, Turkey*

(*Received 00 Month 20XX; final version received 00 Month 20XX*)

A coupled Weakly Compressible (WC) and Total Lagrangian (TL) Smoothed Particle Hydrodynamics (SPH) method is developed for simulating hydroelastic problems. The fluid phase is simulated using WCSPH method while the structural dynamics are solved using TLSPH method. Fluid and solid components of the method are introduced and validated separately. A sloshing water tank problem is solved to test the WCSPH method while oscillation of a thin plate and large deformation of a cantilever beam are simulated to test TLSPH method. After validating each component, the coupled WC-TL SPH scheme is introduced and two benchmark hydroelastic problems are simulated. The first test case shows the evolution of water column with an elastic boundary gate, and the second one investigates the breaking water column impact on elastic structures. The agreement between WC-TL SPH results and literature data shows the ability of the proposed method in simulating hydroelastic phenomena.

Keywords: Hydroelasticity; Fluid-Structure Interaction; Smoothed Particle Hydrodynamics; Weakly Compressible SPH; Total Lagrangian SPH; Particle Methods

1. Introduction

Structures interacting with free surface flows are of great interest in many engineering applications such as ship dynamics, marine hydrodynamics and offshore structure design. In some cases, the deformation of the solid phase is small enough to be neglected and the structure is modeled as a rigid body. However, when the deformation in the solid phase is comparable to the scale of the system, the structure has to be fully resolved to capture the correct behavior of the system. One such case, referred to as hydroelastic problem, is the interaction of elastic bodies with free surface

*Corresponding author. Email: ntofighi@uvic.ca

E-mails: JH (chrishe1900@gmail.com) MY (meyildiz@sabanciuniv.edu) JL (leijm@bit.edu.cn) AS (suleman@uvic.ca)

flows. Some experimental studies in hydroelastic problems are conducted by Hermundstad (1995), Stenius et al. (2013), Panciroli and Porfiri (2015) and Wang et al. (2016).

Developing robust and efficient numerical methods to simulate the hydroelastic problem has been the focus of many works. A large number of these methods are grid-based schemes, relying on body-fitted meshes (Bathe, Zhang, and Ji 1999; Lu, He, and Wu 2000; Czygan and von Estorff 2002; Hubner, Walhorn, and Dinkler 2004; Liao and Hu 2013). However, body-fitted grid-based methods require complicated remeshing and mesh movement schemes to track large deformations. Lagrangian meshless methods provide alternatives that capture such deformations naturally, making them suitable for simulating free surface flows and interactions with highly deformable structures. Smoothed particle hydrodynamics (SPH), first proposed by Gingold and Monaghan (1977) and Lucy (1977), is one of the most popular meshless methods.

SPH has been successfully used to simulate free surface flow problems, including dam-break (Monaghan 1994; Colagrossi and Landrini 2003; Adami, Hu, and Adams 2012) and sloshing motion (Faltinsen et al. 2000). Rigid body motion has also been the subject of many studies (Oger et al. 2006; Shao 2009; Skillen et al. 2013; Sun, Ming, and Zhang 2015; Tofighi et al. 2015). Oger et al. (2006) and Shao (2009) studied the slamming motion of a rigid wedge on a quiescent free surface. Interaction of rigid bodies with quiescent and wavy flow surfaces (Skillen et al. 2013; Sun, Ming, and Zhang 2015) as well as their sedimentation (Sun, Ming, and Zhang 2015; Tofighi et al. 2015) have also been studied.

SPH method is also employed in elastic dynamic problems (Libersky et al. 1993; Gray, Monaghan, and Swift 2001; Maurel and Combescure 2008; Potapov et al. 2009; Caleyron et al. 2013). Antoci, Gallati, and Sibilla (2007) used a Weakly Compressible SPH (WCSPH) based numerical algorithm for solving hydroelastic problems. In their work, both fluid and solid phases are simulated using WCSPH. However, tensile instability limits the application of WCSPH in elastic dynamic problems (Swegle, Hicks, and Attaway 1995; Swegle 2000). While tensile instability is encountered in both fluid and solid phases, the effect is much more pronounced for elastic bodies (Gray, Monaghan, and Swift 2001). Many remedies, including normalizing interpolation kernels (Johnson and Beissel 1996) and applying artificial stress (Antoci, Gallati, and Sibilla 2007), were used to reduce the effects of tensile instability. However, these techniques add additional model parameters that have to be chosen carefully (Morris 1996). On the other hand, SPH-FEM was used as an alternative approach (Fourey et al. 2010; Groenenboom and Cartwright 2010; Panciroli et al. 2012; Yang, Jones, and McCue 2012; Panciroli, Abrate, and Minak 2013; Li et al. 2015). In SPH-FEM, SPH method is only used to simulate the fluid domain while the solid domain is simulated using Finite Element Method (FEM). SPH-FEM is a highly regarded method and has been successfully used to simulate several cases in hydroelasticity. However, the different requirements of its solid and fluid solver modules result in complex coupling procedures. A method fully based on SPH discretization is less complex as the modules share common routines and particles have similar meaning across both solid and fluid solver modules.

In their stability analysis of meshless particle methods, Belytschko et al. (2000) suggested a Total Lagrangian Formulation of SPH (TLSPH) for elastic dynamic problems. In this method, the initial configuration is used as a reference and kernel function and its derivatives are calculated based on the initial particle distribution (Bonet and Kulasegaram 2001; Vidal, Bonet, and Huerta 2007). Unlike WCSPH method used by Gray, Monaghan, and Swift (2001) and Antoci, Gallati, and Sibilla (2007), Hook's law relates stress to strain directly in TLSPH and no artificial equation of state is required. Results show that TLSPH method alleviates the tensile instability problem without additional treatments (Lin et al. 2014, 2015).

The motivation behind this work is to develop a Weakly Compressible and Total Lagrangian SPH (WC-TL SPH) framework to simulate hydroelastic problems. To this end, we base our fluid solver on WCSPH method by Monaghan (2005) while the elastic dynamic problem is solved using TLSPH method proposed by Lin et al. (2014). The boundary conditions on fluid boundaries are imposed via dummy particles (Adami, Hu, and Adams 2012). These boundary particles double as solid particles inside the elastic bodies, providing seamless transition between fluid and solid regions. The combination provides an easy to implement and efficient method with natural coupling between fluid and solid solvers.

In order to validate the proposed method, individual elements of the scheme are tested separately first. A sloshing water tank problem is used to test the WCSPH implementation while oscillation of a thin plate and large deformation of a cantilever beam are used to validate the TLSPH scheme. Two test cases, an elastic plate subject to transient water pressure and breaking water column impact on an elastic obstacle, are then considered for the validation of the coupled WC-TL SPH scheme. The results are in good agreement with experimental and numerical data available in literature, showing the ability of the proposed method in simulating hydroelastic problems. The rest of the paper is arranged as follows. WCSPH and TLSPH schemes are presented in sections 2 and 3, respectively, while the coupling method is outlined in section 4. Simulation results are validated in section 5 and concluding remarks are drawn in section 6.

2. WCSPH formulation for free surface flows

2.1. *Governing equations*

In this paper, we assume the fluid to be non-viscous. The shear stresses are neglected, and we reduce the Navier-Stokes equations into Euler equations,

$$\frac{\mathrm{d}\rho}{\mathrm{d}t} = \rho \boldsymbol{\nabla} \cdot \mathbf{v}, \tag{1}$$

$$\frac{\mathrm{d}\mathbf{v}}{\mathrm{d}t} = -\frac{1}{\rho}\boldsymbol{\nabla} p + \mathbf{g}, \tag{2}$$

with ρ, $\mathbf{v}$, p, t and $\mathbf{g}$ denoting density, velocity vector, pressure, time and gravity. In all cases considered here, $\mathbf{g}$ points downward and has a magnitude of $9.8m/s^2$.

Following the WCSPH scheme to simulate incompressible fluids (Monaghan 1994), a state equation of the form

$$p = p_0 \left[\left(\frac{\rho}{\rho_0} \right)^{\gamma} - 1 \right] \tag{3}$$

is employed, where $\gamma = 7$ for water while p_0 and ρ_0 are reference pressure and density, with $p_0 = \rho_0 g H$ and H is the maximum depth the of fluid.

2.2. *Numerical scheme*

The fundamental concept of SPH is an interpolation process (Gingold and Monaghan 1977; Lucy 1977) and spatial derivatives are determined by relating the particle of interest and the neighboring particles through a kernel function.

The discretized form of continuity equation and momentum equations (Monaghan 2005) for a fluid particle i may be written as

$$\frac{\mathrm{d}\rho_{\mathrm{i}}}{\mathrm{d}t} = \rho_{\mathrm{i}} \sum_{\mathrm{j}} \frac{m_{\mathrm{j}}}{\rho_{\mathrm{j}}} \left(\mathbf{v}_{\mathrm{j}} - \mathbf{v}_{\mathrm{i}} \right) \boldsymbol{\nabla} W_{\mathrm{ij}}, \tag{4}$$

$$\frac{\mathrm{d}\mathbf{v}_{\mathrm{i}}}{\mathrm{d}t} = -\sum_{\mathrm{j}} m_{\mathrm{j}} \left(\frac{p_{\mathrm{i}}}{\rho_{\mathrm{i}}^2} + \frac{p_{\mathrm{j}}}{\rho_{\mathrm{j}}^2} + \Pi_{\mathrm{ij}} \right) \boldsymbol{\nabla} W_{\mathrm{ij}} + \mathbf{g}, \tag{5}$$

where m denotes particle mass and W_{ij} is the shorthand notation for the kernel function $W\left(\left|\mathbf{r}_{\mathrm{j}} - \mathbf{r}_{\mathrm{i}}\right|, h\right)$. Here $\mathbf{r}_{\mathrm{i}}$ is the position vector of particle i while h is the smoothing length, taken 1.33 times of the particle spacing δ_p. In this paper, we use a Gaussian kernel with a compact support of $3h$ (Monaghan 1994).

To maintain the numerical stability of the scheme, an additional artificial viscosity term Π_{ij} is introduced in the momentum equation. Among various formulations of this term in literature, we choose the following form (Monaghan and Gingold 1983)

$$\Pi_{\mathrm{ij}} = \begin{cases} -\alpha \dfrac{\mu_{\mathrm{ij}} c_f}{\bar{\rho}_{\mathrm{ij}}}, & (\mathbf{v}_{\mathrm{j}} - \mathbf{v}_{\mathrm{i}}) \cdot (\mathbf{r}_{\mathrm{j}} - \mathbf{r}_{\mathrm{i}}) < 0 \\ 0, & (\mathbf{v}_{\mathrm{j}} - \mathbf{v}_{\mathrm{i}}) \cdot (\mathbf{r}_{\mathrm{j}} - \mathbf{r}_{\mathrm{i}}) \geq 0 \end{cases} \tag{6}$$

$$\mu_{\mathrm{ij}} = \frac{h\left(\mathbf{v}_{\mathrm{j}} - \mathbf{v}_{\mathrm{i}}\right) \cdot \left(\mathbf{r}_{\mathrm{j}} - \mathbf{r}_{\mathrm{i}}\right)}{\left|\mathbf{r}_{\mathrm{j}} - \mathbf{r}_{\mathrm{i}}\right|^2 + 0.01h^2}, \tag{7}$$

where $\bar{\rho}_{\mathrm{ij}}$ is the average density of particles i and j. Dissipation coefficient α and sound speed in fluid c_f are set to 0.1 and $10\sqrt{gH}$, respectively. A similar stabilizing term based on Π_{ij} is used for solid particles and will be detailed in section 3.2.

The boundary conditions are imposed through the dummy particle approach given by Adami, Hu, and Adams (2012). The pressure of dummy particles, coinciding with either rigid walls or elastic bodies, may be interpolated using the neighboring fluid particle values through

$$p_{\mathrm{d}} = \frac{1}{\sum_{\mathrm{f}} W_{\mathrm{df}}} \left[\sum_{\mathrm{f}} p_{\mathrm{f}} W_{\mathrm{df}} + (\mathbf{g} - \mathbf{a}_s) \cdot \sum_{\mathrm{f}} \rho_{\mathrm{f}} \left(\mathbf{r}_{\mathrm{f}} - \mathbf{r}_{\mathrm{d}}\right) W_{\mathrm{df}} \right], \tag{8}$$

where subscripts d and f denote dummy and fluid particles while $\mathbf{a}_s$ is the acceleration of the solid particles. The density of dummy particles may be calculated from their pressure by

$$\rho_{\mathrm{d}} = \rho_0 \left(\frac{p_{\mathrm{d}}}{p_0} + 1 \right)^{\frac{1}{\gamma}}. \tag{9}$$

In this paper, free-slip boundary condition is implemented in all test cases and the velocity of dummy particles are set equal to the solid particle velocity v_s.

3. TLSPH formulation for elastic dynamics

3.1. *Governing equations*

The governing equations for elastic dynamics are

$$\frac{\mathrm{d}\rho}{\mathrm{d}t} = -\rho \boldsymbol{\nabla} \cdot \mathbf{v}, \tag{10}$$

$$\frac{\mathrm{d}\mathbf{v}}{\mathrm{d}t} = \frac{1}{\rho}\boldsymbol{\nabla}\cdot\boldsymbol{\sigma} + \mathbf{g}, \tag{11}$$

where ρ, $\mathbf{v}$, $\boldsymbol{\sigma}$ and $\mathbf{g}$ denote the density, velocity vector, Cauchy stress tensor and gravity.

3.2. *Numerical scheme*

In this study, the TLSPH method is used to simulate the elastic dynamic problem. This method eliminates the tensile instability problem observed in direct application of SPH for simulation of elastic bodies (Vidal, Bonet, and Huerta 2007; Bonet and Kulasegaram 2001). TLSPH method is more efficient than conventional SPH as kernel function and its gradients are only computed at the beginning of the simulation (Lin et al. 2014). Density is assumed to be constant, eliminating the need for solving the continuity equation (Eq. (10)). To solve the momentum equation (Eq. (11)) in the reference frame, Cauchy stress tensor $\boldsymbol{\sigma}$ is replaced with the first Piola-Kirchhoff stress tensor $\mathbf{P}$, resulting in the following form

$$\frac{\mathrm{d}\mathbf{v}}{\mathrm{d}t} = \frac{1}{\rho_0}\boldsymbol{\nabla}_0\cdot\mathbf{P} + \mathbf{g}, \tag{12}$$

where a subscript $\square_0$ denotes values in initial configuration. The relation between $\mathbf{P}$ and $\boldsymbol{\sigma}$ may be written as

$$\mathbf{P} = \det\left(\mathbf{F}\right)\boldsymbol{\sigma}\mathbf{F}^{-1}, \tag{13}$$

where $\mathbf{F}$ is the deformation gradient tensor, approximated as

$$\mathbf{F}_{\mathrm{i}} = \left(\frac{\mathrm{d}\mathbf{x}}{\mathrm{d}\mathbf{X}}\right)_{\mathrm{i}} = \sum_{\mathrm{j}}\left(\mathbf{x}_{\mathrm{j}} - \mathbf{x}_{\mathrm{i}}\right)\boldsymbol{\nabla}_0 W_{\mathrm{ij}} A_{0\mathrm{j}}. \tag{14}$$

Here $\mathbf{x}$ and $\mathbf{X}$ denote the current and original coordinate vectors, respectively, while $\boldsymbol{\nabla}_0 W_{\mathrm{ij}}$ is kernel gradient corresponding to particle i and j in their original configuration. $A_{0\mathrm{j}}$ denotes the original area of particle j for a 2D problem.

Cauchy stress tensor $\boldsymbol{\sigma}$ may be computed from Euler strain tensor $\boldsymbol{\varepsilon}$ according to Hooke's law for isotropic elastic materials in two dimensions as

$$\begin{bmatrix}\sigma^{11}\\ \sigma^{22}\\ \sigma^{12}\end{bmatrix} = \frac{E}{1-\nu^2}\begin{bmatrix}1 & \nu & 0\\ \nu & 1 & 0\\ 0 & 0 & 1-\nu\end{bmatrix}\begin{bmatrix}\varepsilon^{11}\\ \varepsilon^{22}\\ \varepsilon^{12}\end{bmatrix} \tag{15}$$

for a plane stress problem and as

$$\begin{bmatrix}\sigma^{11}\\ \sigma^{22}\\ \sigma^{12}\end{bmatrix} = \frac{E}{\left(1+\nu\right)\left(1-2\nu\right)}\begin{bmatrix}1-\nu & \nu & 0\\ \nu & 1-\nu & 0\\ 0 & 0 & 1-2\nu\end{bmatrix}\begin{bmatrix}\varepsilon^{11}\\ \varepsilon^{22}\\ \varepsilon^{12}\end{bmatrix} \tag{16}$$

for a plane strain problem. Here, ν and E denote Poisson's ratio and Young's modulus, respectively, while Euler strains may be defined using the deformation gradient as

$$\boldsymbol{\varepsilon} = \mathbf{F}^{-T}\mathbf{E}\mathbf{F}^{T}. \tag{17}$$

Here, $\mathbf{E}$ is Green-Lagrange strain tensor expressed as

$$\mathbf{E} = \frac{1}{2}\left[\mathbf{L} + \mathbf{L}^T + \mathbf{L}^T\mathbf{L}\right], \tag{18}$$

where the third term on the right hand side takes the geometrical non-linear effects into consideration. In the above equation, displacement gradient tensor $\mathbf{L}$ at particle i is defined according to displacement vector $\mathbf{u}$ as

$$\mathbf{L}_\mathrm{i} = \left(\frac{\mathrm{d}\mathbf{u}}{\mathrm{d}\mathbf{X}}\right)_\mathrm{i} = \sum_\mathrm{j}\left(\mathbf{u}_\mathrm{j} - \mathbf{u}_\mathrm{i}\right)\boldsymbol{\nabla}_0 W_\mathrm{ij} A_{0\mathrm{j}}. \tag{19}$$

The momentum equation in reference configuration (Eq. (12)) may be rewritten in its discretized form as (Lin et al. 2014, 2015)

$$\frac{\mathrm{d}\mathbf{v}_\mathrm{i}}{\mathrm{d}t} = -\sum_\mathrm{j}\left(\frac{\mathbf{P}_\mathrm{i}}{\rho_{0\mathrm{i}}^2} + \frac{\mathbf{P}_\mathrm{j}}{\rho_{0\mathrm{j}}^2} + \mathbf{P}_{\nu\mathrm{ij}}\right)\boldsymbol{\nabla}_0 W_{0\mathrm{ij}}\rho_{0\mathrm{j}}A_{0\mathrm{j}} + \mathbf{g}. \tag{20}$$

Here, $\mathbf{P}_\nu$ is the artificial viscous term Π_ij between particles i and j (Eq. (6)) transformed to reference coordinates as

$$\mathbf{P}_{\nu\mathrm{ij}} = \det\left(\mathbf{F}\right)\Pi_\mathrm{ij}\mathbf{F}^{-1}, \tag{21}$$

where the sound speed in fluid c_f is replaced with sound speed in solid $c_s = \sqrt{E/\rho_0}$.

4. WC-TL SPH coupling scheme

In sections 2 and 3, the WCSPH algorithm for free surface flow simulations and TLSPH algorithm for solving elastic dynamic problems were introduced separately. In this section, we present the coupled WC-TL SPH scheme employed in solving hydroelastic problems. A typical particle arrangement for a hydroelastic simulation using the coupled WC-TL SPH method is illustrated in Fig. 1. The figure shows fluid particles, dummy particles and solid particles. The solid particles shown in the figure also act as dummy particles for imposing boundary conditions on the fluid particles in the vicinity of the solid body. The dummy particles residing at the outer layer of the solid body, referred to as interface particles and shown by the solid line in Fig. 1, are used to transfer the fluid pressure force to the solid.

Fig. 2 specifies the details of the proposed WC-TL SPH scheme. At the beginning, particle coordinates, properties and velocities are initialized. Then the main computational routine is executed. Assuming the routine is executing the time step $(n+1)$, WCSPH solver is used to update the fluid particle coordinates, velocities and pressures explicitly using the values of (n)th time step. Boundary conditions are applied through dummy particles where their pressure and velocity are computed through Eqs. (8) and (9). At this stage both interface and solid particles as well as wall boundary particles function as dummy particles. Denoting the pressure computed at interface particle k as p_k, an equivalent interfacial force $\mathbf{f}_{(i)\mathrm{k}}$ may be defined as

$$\mathbf{f}_{(i)\mathrm{k}}^{(n)} = \left[p_\mathrm{k}\Delta s_\mathrm{k}\hat{\mathbf{n}}_\mathrm{k}\right]^{(n)}. \tag{22}$$

Here, $\square^{(n)}$ denotes (n)th time step while $\hat{\mathbf{n}}_\mathrm{k}$ is unit normal at particle k, excluding corner particles.

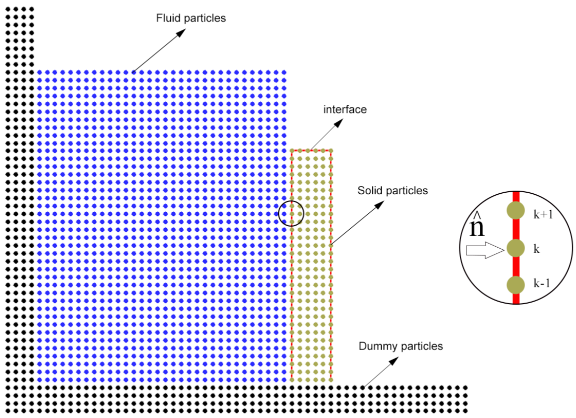

Figure 1. Schematic diagram of the coupled WC-TL SPH scheme. The inset shows the interface particle positions.

For adjacent interface particles $\mathrm{k}-1$, k and $\mathrm{k}+1$, Δs_{k} is approximated as

$$\Delta s_{\mathrm{k}}^{(n)} = \left[\frac{1}{2}\left|\mathbf{x}_{\mathrm{k}} - \mathbf{x}_{\mathrm{k}-1}\right| + \frac{1}{2}\left|\mathbf{x}_{\mathrm{k}+1} - \mathbf{x}_{\mathrm{k}}\right|\right]^{(n)}. \tag{23}$$

The interfacial force $\mathbf{f}_{(i)}$ is applied to the solid body as a boundary condition while calculating the elastic dynamic problem using TLSPH method. This concludes one routine of the WC-TL SPH method at the current time step. While executing the fluid solver at the next time step $(n+2)$, the updated accelerations, velocities and coordinates of the solid and interface particles at the time step $(n+1)$ are used in dummy particle calculations.

The force balance of interface particles is fulfilled through Eq. (8). For a detailed derivation and extensive validation of this boundary condition, the reader is referred to the work by Adami, Hu, and Adams (2012). The above mentioned routine is a one-way coupling and thus imposes strict time stepping requirements. To ensure the accuracy of the solution across solid and fluid solvers, the time step is chosen according to Courant-Friedrichs-Lewy condition (Lin et al. 2015; Adami, Hu, and Adams 2012),

$$\Delta t^{(n)} = \min\left(0.8\frac{h}{c_s}, 0.25\frac{h}{c_f + v_{\max}^{(n)}}, 0.25\sqrt{\frac{h}{g}}\right) \tag{24}$$

where $v_{\max}$ is the magnitude of maximum fluid velocity inside the domain. Sound speed in fluid $c_f = 10\sqrt{gH}$ and sound speed in solid $c_s = \sqrt{E/\rho_0}$ are defined in sections 2.2 and 3.2, respectively.

5. Results

In this section, the results of the proposed WC-TL SPH scheme are validate against numerical and experimental data available in the literature. First, a sloshing water tank problem is solved to test the WCSPH implementation. Then the TLSPH implementation is validated by simulating the oscillation of a thin plate and large deformation of a cantilever beam and comparing the results with analytical and numerical data. Finally, the coupled WC-TL SPH is used to simulate two cases, an elastic plate subject to transient water pressure and breaking water column impact on an elastic obstacle, and the results are compared to those available in the literature.

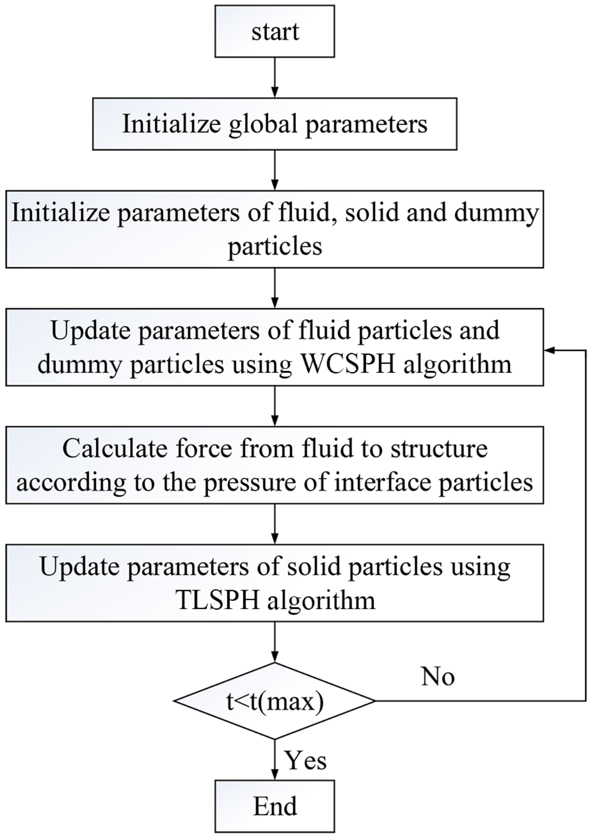

Figure 2. Flowchart of the coupled WC-TL SPH scheme.

5.1. *Sloshing water tank under horizontal excitation*

In this example, we simulated the water's movement in a sloshing rectangular tank. The length and height of the tank are $L = 1.73m$ and $H = 1.15m$, respectively, while the water depth is $h_w = 0.6m$. The tank moves in horizontal direction according to $S = A\cos(2\pi t/T)$, where S is the location of the tank, and A is the amplitude and T is the period. The velocity and acceleration of the wall dummy particles are computed from S. Following Faltinsen et al. (2000), we choose $A = 0.032m$ and $T = 1.3s$. Fig. 3 shows the initial particle distribution for this case with an initial particle spacing of $\delta_p = 0.01m$, which leads to 10380 fluid particles and 1644 dummy particles. Fig. 4 shows nine snapshots of pressure contours and surface profiles from $t = 1.0s$ to $t = 9.0s$ at $1.0s$ intervals.

Fig. 5 plots the wave height $0.05m$ away from the left wall inside the tank versus time against experimental data by Faltinsen et al. (2000). We simulated this case with particle spacings of $\delta_p = 0.02m$, $0.01m$ and $0.005m$ which leads to 30, 60 and 120 particles in vertical direction. The results converge for $\delta_p \leq 0.01$ and show good agreement with the experimental data.

5.2. *Oscillating plate*

In order to validate the accuracy of TLSPH algorithm in solving transient linear elastic dynamic problems, the oscillation of a thin cantilever plate is simulated. Fig. 6 shows the geometry of the plate. The plate length is $L = 0.2m$ and the height is $H = 0.02m$. When initialized with a velocity

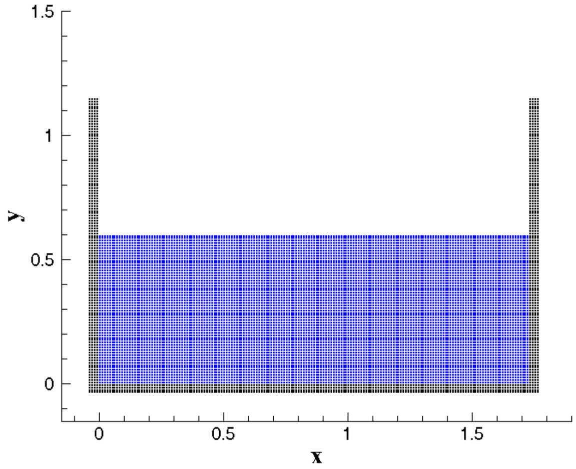

Figure 3. Initial particle distribution of a water tank.

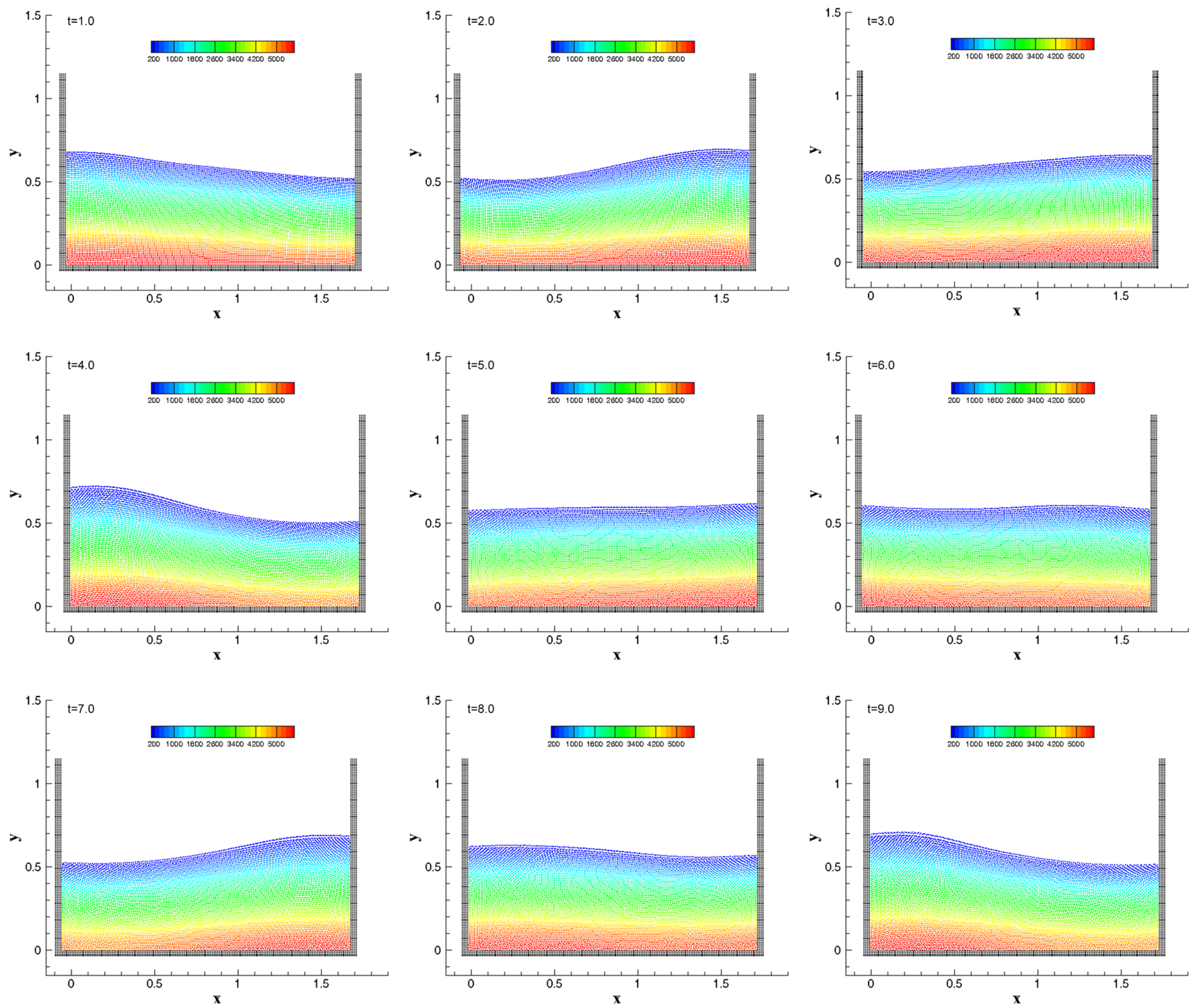

Figure 4. Contours of pressure and free surface profiles for sloshing motion. Snapshots are taken at 1.0s intervals from $t = 1.0s$ (top-left) to $t = 9.0s$ (bottom-right).

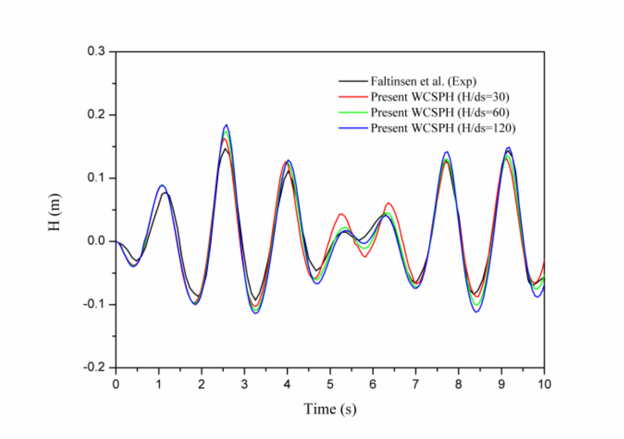

Figure 5. Comparison of wave heights between WCSPH and experimental results.

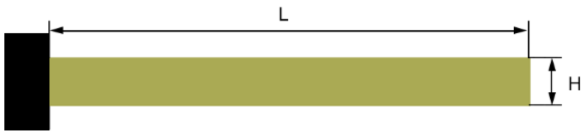

Figure 6. Initial geometry of the plate.

of the form

$$v_y(x) = v_L c_0 \frac{f(x)}{f(L)}, \tag{25}$$

where

$$\begin{aligned} f(x) = &(\cos kL + \cosh kL)(\cosh kx - \cos kx) \\ &+ (\sin kl - \sinh kl)(\sinh kx - \sin kx), \end{aligned} \tag{26}$$

a thin plate with one clamped end and one free end will oscillate with a fundamental frequency of ω (Gray, Monaghan, and Swift 2001), given as

$$\omega^2 = \frac{EH^2k^4}{12\rho(1-\nu^2)}, \tag{27}$$

where $kL = 1.875$. The initial velocity of the free end is set to $v_L = 0.01$ and the speed of sound is $c_0 = \sqrt{K/\rho}$. Here K is the bulk modulus of the plate. Following Gray, Monaghan, and Swift (2001), Antoci, Gallati, and Sibilla (2007) and Rafiee and Thiagarajan (2009), the properties of the plate are set to $\rho = 1000kg/m^3$, $K = 3.25 \times 10^6 N/m^2$, $\nu = 0.3975$ and $E = 1.998 \times 10^6 N/m^2$ for comparison.

For resolution test, we choose particle spacings of $\delta_p = 0.002m$, $0.001m$ and $0.0005m$ which correspond to 10, 20 and 40 particles in vertical direction. The simulation results are compared with analytical and numerical data of Gray, Monaghan, and Swift (2001), Antoci, Gallati, and Sibilla (2007) and Rafiee and Thiagarajan (2009) in Fig. 7 and Tab. 1. The plate tip's vertical displacement in Fig. 7 shows that our simulation is well-resolved for $H/\delta_p \geq 20$. The difference between TLSPH results and analytical data shown in Tab. 1, especially for oscillation period, is smaller than numerical simulations given in the literature.

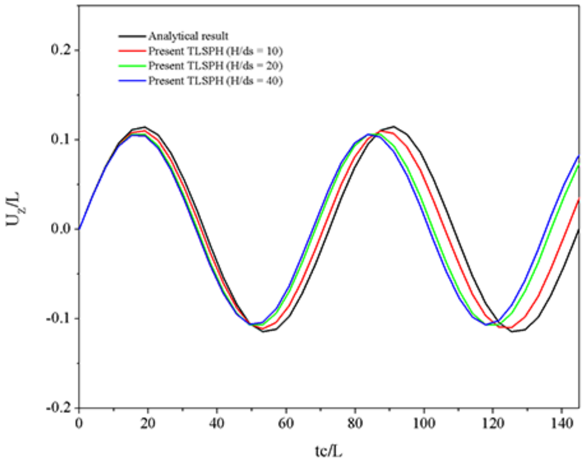

Figure 7. Comparison of non-dimensional vertical displacement versus non-dimensional time.

Table 1. Comparison of non-dimensional period and amplitude for $H = 0.02m$. Error column shows the difference between the given value and the analytical result.

	Period		Amplitude	
	tc/L	Error	A/L	Error
Analytical Solution	72.39	–	0.115	–
TLSPH ($H/\delta_p = 10$)	70.68	2.36%	0.111	3.48%
TLSPH ($H/\delta_p = 20$)	68.4	5.51%	0.108	6.09%
TLSPH ($H/\delta_p = 40$)	67.64	6.56%	0.107	6.96%
Antoci, Gallati, and Sibilla (2007)	81.5	12.58%	0.124	7.83%
Gray, Monaghan, and Swift (2001)	82	13.27%	0.125	8.7%
Rafiee and Thiagarajan (2009)	82.2	13.55%	0.126	9.57%

5.3. *Large deformation of a cantilever beam*

In order to validate our TLSPH code in simulating geometrically nonlinear problems, we studied the large deflection of a cantilever beam under vertical end load (Lin et al. 2014). Unlike the plane strain problem of section 5.2, the cantilever beam studied here is a plane stress problem. The beam has a length of $L = 0.1m$, a height of $H = 0.01m$ and a thickness of $b = 0.001m$. The tip load on the center of the free end is increased linearly from $F = 0$ at $t = 0s$ to $F = -17.5kN$ at $t = 1.0s$ and kept constant until $t = 2.0s$. The beam's Young's modulus E, Poisson's ratio ν and density ρ are set to $210GPa$, 0.3 and $7800kg/m^3$, respectively.

Due to highly nonlinear nature of this problem, analytical solutions are not readily available. As such, we compare our results with those obtained from Abaqus software. Figs. 8 and 9 show the deformed configurations where our results and Abaqus data are in close agreement. Fig. 10 plots the time history of horizontal and vertical displacements obtained by TLSPH method and Abaqus. It is seen that both solutions reach a steady state at $t = 1.0s$, producing similar horizontal and vertical displacements.

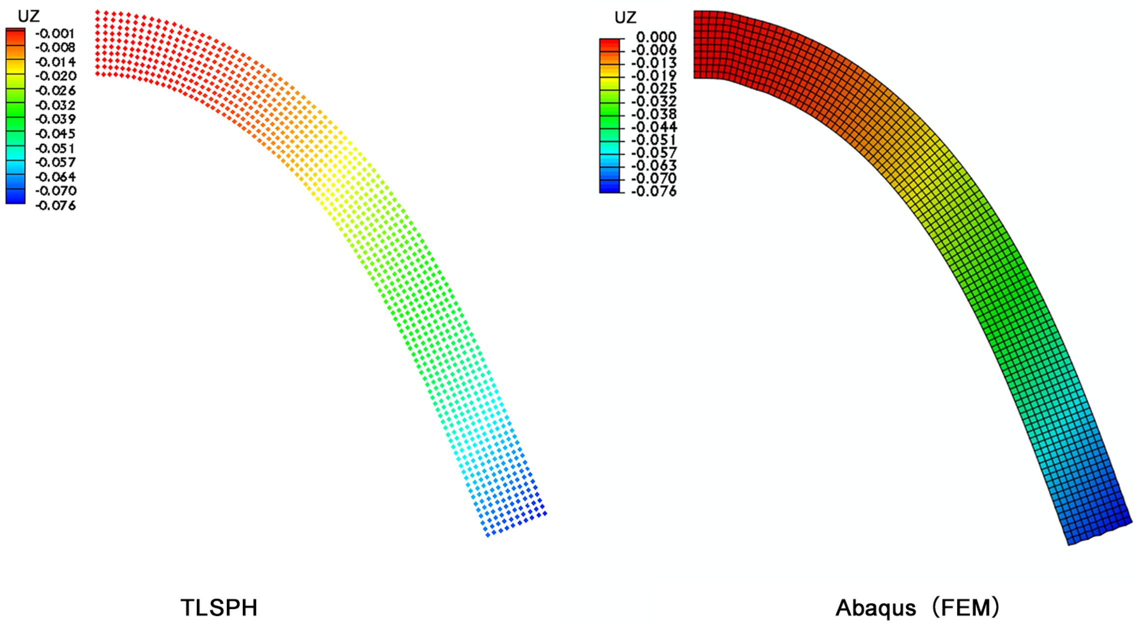

Figure 8. Comparison of TLSPH and FEM results of the deformed beam at $t = 0.5s$ (colored by vertical displacement).

5.4. *An elastic plate subjected to transient water pressure*

The deformation of an elastic plate under water pressure was studied by Antoci, Gallati, and Sibilla (2007) experimentally and numerically. Fig. 11 shows the initial configuration of the system. The water column has a width of $0.1m$ and a height of $0.14m$ where the top side is a free surface at ambient conditions. All other sides are walls where an elastic plate covers the lower portion of the right wall. The elastic plate, with a width of $0.005m$ and a height of $0.079m$, is fixed at the top and is initially straight. The density of water is set to $\rho_f = 1000kg/m^3$. The material of the elastic plate is rubber with density $\rho_s = 1100kg/m^3$, Young's modulus $E = 10^6 Pa$ and Poisson's ratio $\nu = 0.4$. Simulations are carried out with particle spacings of $0.001m$, $0.0005m$ and $0.00033m$ corresponding to 31374, 62744 and 94120 particles in total, including fluid, solid and dummy particles. The CPU-times on an Intel Core i5-4460/3.2GHz computer are 7, 55.5 and 169.7 hours to reach $0.4s$ simulation time for the above cases. The results (not shown here) indicate that an initial particle spacing of $0.0005m$ provides sufficient accuracy and further comparison with literature data is carried on using this resolution.

Fig. 12 shows contours of water pressure and σ_{yy} in elastic plate at $0.04s$ intervals starting from $t = 0.04s$. Similar behavior has been observed by Antoci, Gallati, and Sibilla (2007) in their experimental work. To quantify our results, we compare the time history of both horizontal and vertical displacements at the free end of the rubber plate with the experimental and other numerical results (Antoci, Gallati, and Sibilla 2007; Yang, Jones, and McCue 2012; Li et al. 2015) in Fig. 13. Antoci, Gallati, and Sibilla (2007) use a hypoelastic material model for the solid while Yang, Jones, and McCue (2012) and Li et al. (2015) use a hyperelastic model. When compared to SPH results by Antoci, Gallati, and Sibilla (2007) and SPH-FEM results by Yang, Jones, and McCue (2012), our results show better agreement with the experimental data and SPH-FEM simulations by Li et al. (2015), especially when the plate reaches its maximum displacement at $t \approx 0.15s$.

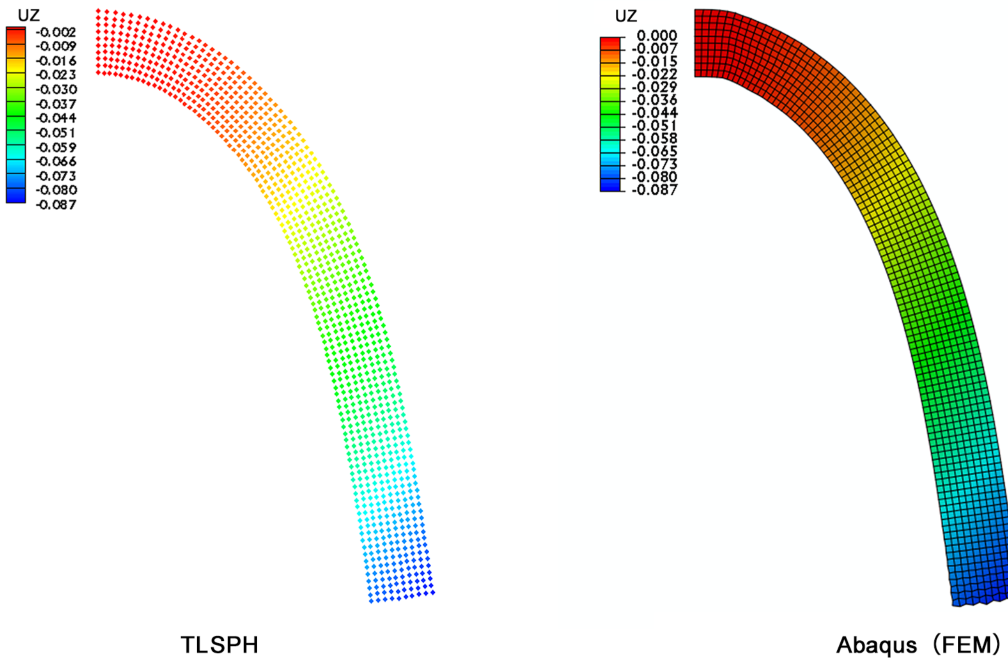

Figure 9. Comparison of TLSPH and FEM results of the deformed beam at $t = 1.0s$ (colored by vertical displacement).

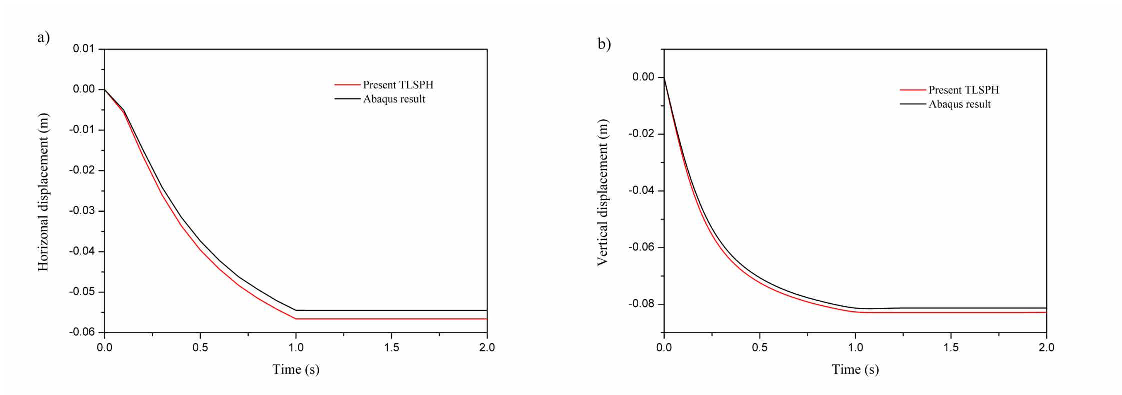

Figure 10. Time history of horizontal (a) and vertical (b) displacements at the free end of the beam.

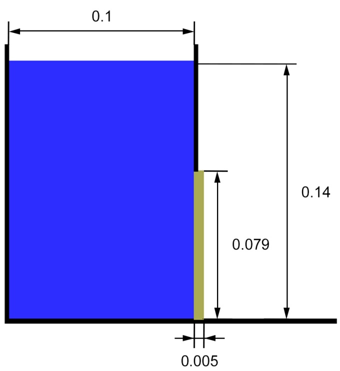

Figure 11. Initial configuration of water column with an elastic plate.

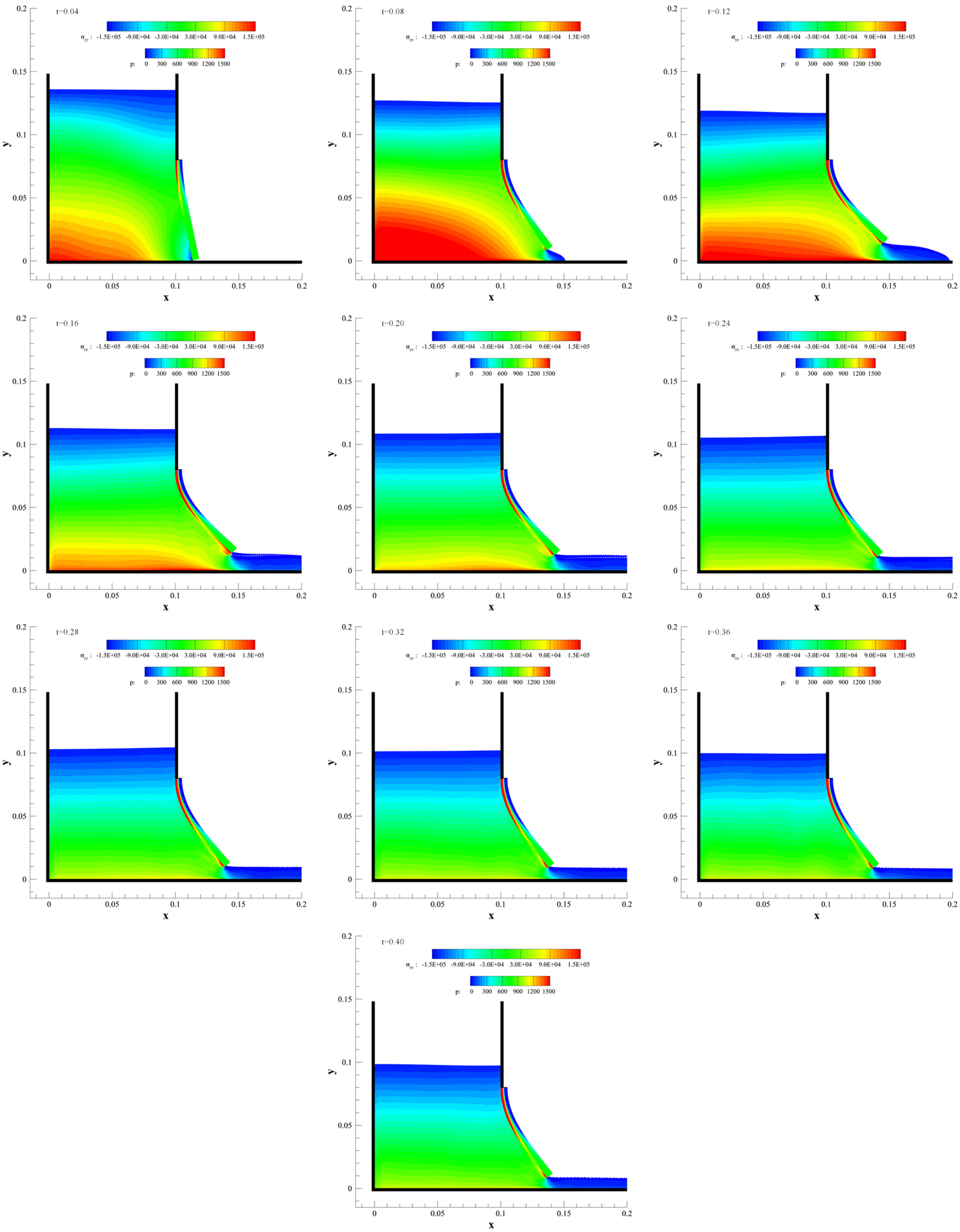

Figure 12. Contours of water pressure and σ_{yy} in the elastic plate. Snapshots are taken at $0.04s$ intervals from $t = 0.04s$ to $0.4s$. Time increases from left to right and top to bottom.

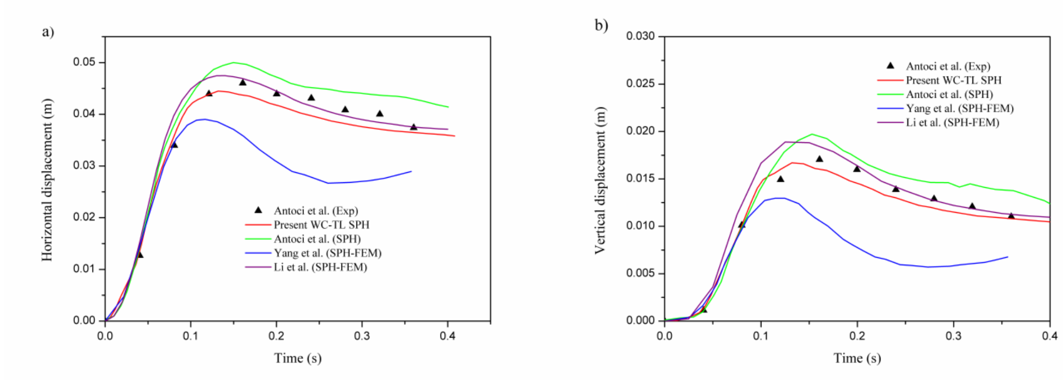

Figure 13. Time history of horizontal (a) and vertical (b) displacements at the free end of the elastic plate.

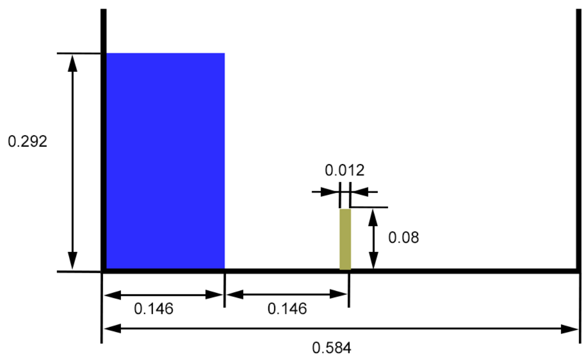

Figure 14. Initial configuration of water column with an elastic obstacle.

5.5. *Breaking water column impact on elastic plate*

The collapse of a water column on an elastic obstacle, a typical hydroelastic problem, is studied in this section. The initial configuration of the system is shown in Fig. 14. A water column with a width of $0.146m$ and a height of $0.292m$ is placed at the left end of a $0.584m \times 0.292m$ container. The $0.08m \times 0.012m$ elastic obstacle is placed in the middle of the container, fixed to the bottom wall at one end and free to move at the other end. The density of water and elastic obstacle are set to $\rho_f = 1000kg/m^3$ and $\rho_s = 2500kg/m^3$. Three test cases with Young's modulus E set to $5 \times 10^5 N/m^2$, $10^6 N/m^2$ and $2 \times 10^6 N/m^2$ are simulated here. For $E = 10^6 N/m^2$, simulations are carried out with particle spacings of $0.0024m$, $0.0012m$ and $0.0008m$ corresponding to 17312, 34640 and 51970 particles. The CPU-times on an Intel Core i5-4460/3.2GHz computer are 5.1, 20.4 and 90.3 hours to reach $0.5s$ simulation time for the above cases. Comparing the results (not shown here), an initial particle spacing of $0.0012m$ is found to be sufficiently accurate and is used for all other cases in this section.

Fig. 15 shows snapshots of water interface and obstacle profiles as well as water pressure for every $0.1s$ starting from $t = 0.1s$ for $E = 10^6 N/m^2$. After its release, the water column collapses and reaches the elastic obstacle. Initially the fluid pressure near the obstacle increases drastically, causing it to deform under the impact of water. Then, as water passes over the obstacle and pressure drops, the obstacle rebounds. Similar behavior is reported in numerical simulations by Hu et al. (2014) and Rafiee and Thiagarajan (2009). Fig. 16 compares the surface profiles for different Young's moduli. At $t = 0.2s$ when the obstacle undergoes considerable deformation, larger Young's modulus results in wider high pressure region. The arc of water passing over the obstacle touches the right wall at a higher point for cases with larger Young's modulus. The lower surface of this arc of water has a wavy pattern for $E = 5 \times 10^6 N/m^2$ at $t = 0.4s$.

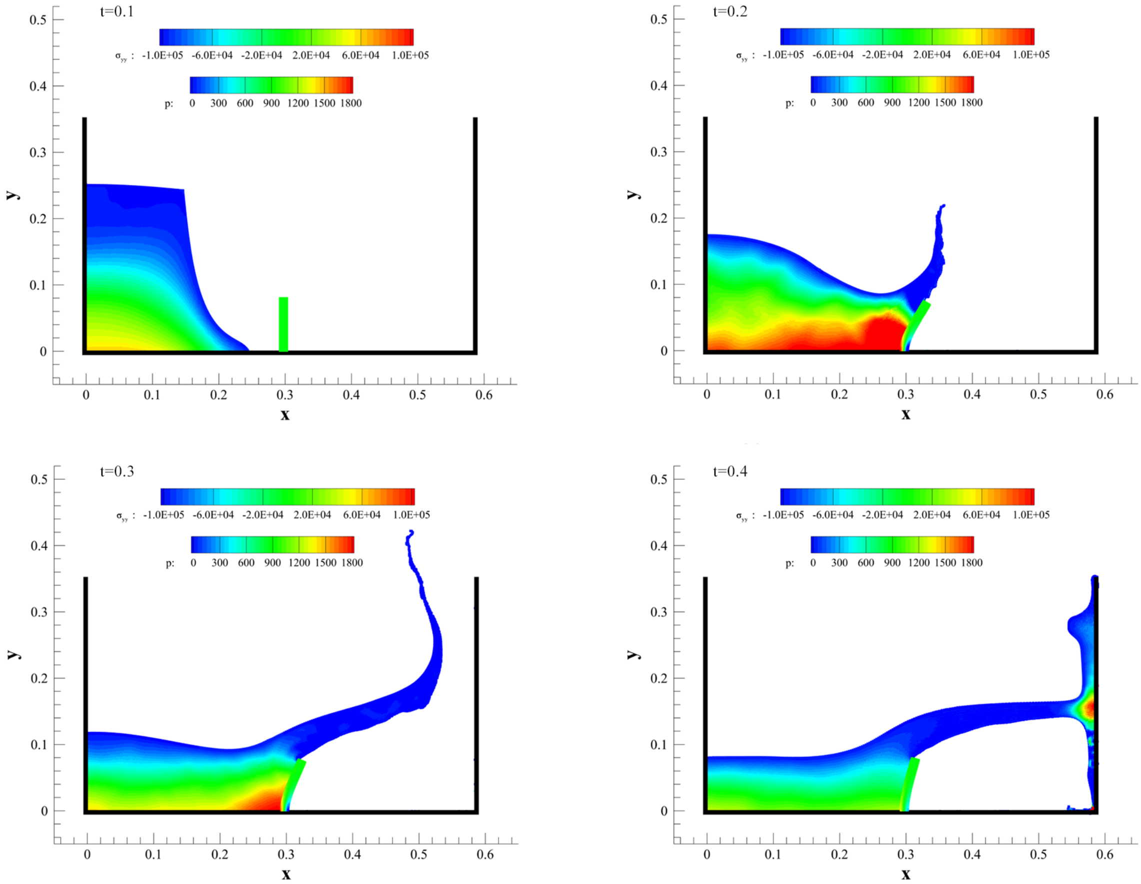

Figure 15. Contours of water pressure, surface profile and σ_{yy} in elastic obstacle. Snapshots are taken at $0.1s$ intervals from $t = 0.1s$ (top-left) to $0.4s$ (bottom-right).

Fig. 17-a plots the time history of displacement of the upper left corner of the obstacle with $E = 10^6 N/m^2$ against numerical results given by Walhorn et al. (2005), Marti et al. (2006), Rafiee and Thiagarajan (2009) and Li et al. (2015). While Walhorn et al. (2005) and Li et al. (2015) use linear elastic solids, Marti et al. (2006) and Rafiee and Thiagarajan (2009) employ a hypoelastic model for their solid material. All simulations follow the same trend, however, the values show some differences. The initial response to the impact starts at $t \approx 0.15s$ and our results are comparable to those of Marti et al. (2006), Rafiee and Thiagarajan (2009) and Li et al. (2015) while the response is slightly delayed in data given by Walhorn et al. (2005). The maximum deflection ($t \approx 0.25s$) and the subsequent rebounding profile of the obstacle are different for all simulations. Our results get closer to the position given by Marti et al. (2006) and Rafiee and Thiagarajan (2009) at later simulation times. In short, the results of the current method are within the range of the data provided in the literature. Fig. 17-b compares the horizontal displacement for different values of Young's modulus. As expected, the cases with lower Young's modulus show larger deformation. The obstacle with $E = 5\times10^5 N/m^2$ exhibits an oscillatory motion while rebounding. This behavior is in agreement with the wavy pattern of the lower surface of water arc seen in Fig. 16.

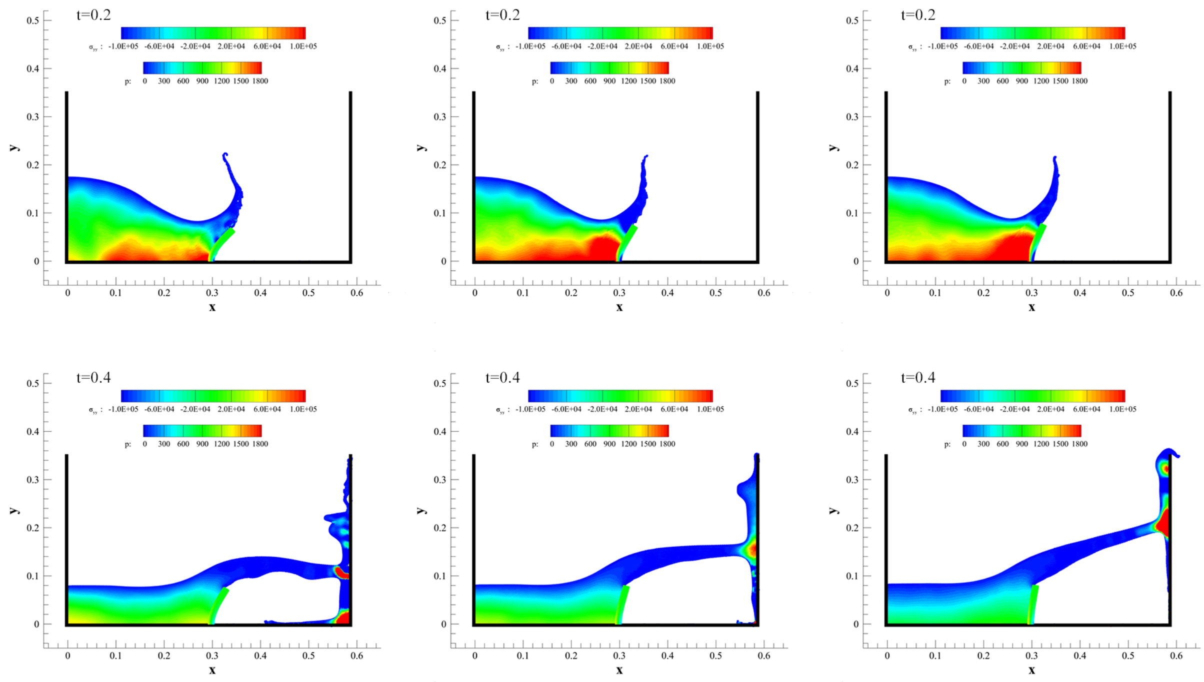

Figure 16. Contours of water pressure, surface profile and von Mises stress in elastic obstacle at $t = 0.2s$ and $t = 0.4s$. (left column) $E = 5 \times 10^5 N/m^2$; (middle column) $E = 10^6 N/m^2$; (right column) $E = 2 \times 10^6 N/m^2$.

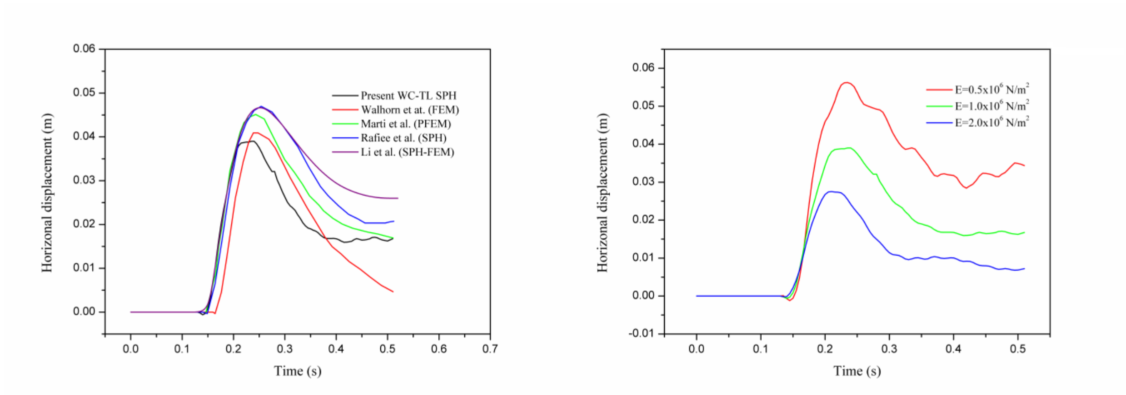

Figure 17. Horizontal displacement history of the upper left corner of the elastic obstacle. (a) comparison with literature data for $E = 10^6 N/m^2$; (b) comparison between cases with different Young's moduli.

6. Conclusion

A coupled Weakly Compressible and Total Lagrangian SPH (WC-TL SPH) method has been developed to simulate the interactions of elastic bodies with free surface flows, known as hydroelastic problems. The fluid phase was simulated by the conventional WCSPH algorithm and the dummy particle method was used to enforce the boundary condition. The solid phase was simulated using the TLSPH method to reduce the tensile instability effect. The particles discretizing the solid phase are used as dummy particles to impose the boundary conditions when fluid particles are close to the elastic body.

The method was validated through five test cases by comparing the numerical result with analytical, experimental and other numerical results available in literature. Our results show that the

WCSPH algorithm can accurately predict the free surface flows and the TLSPH method works well in simulating the transient geometrical nonlinear elastic dynamic problems. The combination, WC-TL SPH, was tested for deformation of an elastic element under different pressure conditions and the results are found to be in agreement with literature data.

The fluid and solid solvers of the WC-TL SPH method are easy to implement and computationally efficient while they couple naturally. The agreement between our results and literature data shows the ability of the proposed method in solving hydroelastic problems.

Funding

JH wishes to acknowledge the financial support from the program of China Scholarship Council under the grant number 201406030037. NT gratefully acknowledges financial support from Mitacs-Accelerate program under the grant number IT08354. MY acknowledges financial support provided by the Scientific and Technological Research Council of Turkey (TUBITAK) for grant number 112M721. AS acknowledges the financial support provided by the Natural Sciences and Engineering Research Council (NSERC) for the Canada Research Chair in Computational and Experimental Mechanics.

References

Adami, S., X. Y. Hu, and N. A. Adams. 2012. "A generalized wall boundary condition for smoothed particle hydrodynamics." *Journal of Computational Physics* 231 (21): 7057–7075.

Antoci, C., M. Gallati, and S. Sibilla. 2007. "Numerical simulation of fluid-structure interaction by SPH." *Computers & Structures* 85 (11-14, SI): 879–890.

Bathe, K. J., H. Zhang, and S. H. Ji. 1999. "Finite element analysis of fluid flows fully coupled with structural interactions." *Computers & Structures* 72 (1-3): 1–16.

Belytschko, T., Y. Guo, W. K. Liu, and S. P. Xiao. 2000. "A unified stability analysis of meshless particle methods." *International Journal for Numerical Methods in Engineering* 48 (9): 1359–1400.

Bonet, J., and S. Kulasegaram. 2001. "Remarks on tension instability of Eulerian and Lagrangian corrected smooth particle hydrodynamics (CSPH) methods." *International Journal for Numerical Methods in Engineering* 52 (11): 1203–1220.

Caleyron, F., A. Combescure, V. Faucher, and S. Potapov. 2013. "SPH modeling of fluid-solid interaction for dynamic failure analysis of fluid-filled thin shells." *Journal of Fluids and Structures* 39: 126–153.

Colagrossi, A., and M. Landrini. 2003. "Numerical simulation of interfacial flows by smoothed particle hydrodynamics." *Journal of Computational Physics* 191 (2): 448–475.

Czygan, O., and O. von Estorff. 2002. "Fluid-structure interaction by coupling BEM and nonlinear FEM." *Engineering Analysis with Boundary Elements* 26 (9): 773–779.

Faltinsen, O. M., O. F. Rognebakke, I. A. Lukovsky, and A. N. Timokha. 2000. "Multidimensional modal analysis of nonlinear sloshing in a rectangular tank with finite water depth." *Journal of Fluid Mechanics* 407: 201–234.

Fourey, G., G. Oger, D. Le Touze, and B. Alessandrini. 2010. "Violent fluid-structure interaction simulations using a coupled SPH/FEM method." In *9th World Congress on Computational Mechanics and 4th Asian Pacific Congress on Computational Mechanics,* Vol. 10 edited by Khalili, N and Valliappan, S and Li, Q and Russell, A.

Gingold, R. A., and J. J. Monaghan. 1977. "Smoothed particle hydrodynamics - theory and application to non-spherical stars." *Monthly Notices of the Royal Astronomical Society* 181 (2): 375–389.

Gray, J. P., J. J. Monaghan, and R. P. Swift. 2001. "SPH elastic dynamics." *Computer Methods in Applied Mechanics and Engineering* 190 (49-50): 6641–6662.

Groenenboom, P. H. L., and B. K. Cartwright. 2010. "Hydrodynamics and fluid-structure interaction by coupled SPH-FE method." *Journal of Hydraulic Research* 48 (SI): 61–73.

Hermundstad, O. A. 1995. "Theoretical and experimental hydroelastic analysis of high speed vessels." Ph.D. thesis. The Norwegian Institute of Technology.

Hu, D., T. Long, Y. Xiao, X. Han, and Y. Gu. 2014. "Fluid-structure interaction analysis by coupled FE-SPH model based on a novel searching algorithm." *Computer Methods in Applied Mechanics and Engineering* 276: 266–286.

Hubner, B., E. Walhorn, and D. Dinkler. 2004. "A monolithic approach to fluid-structure interaction using space-time finite elements." *Computer Methods in Applied Mechanics and Engineering* 193 (23-26): 2087–2104.

Johnson, G. R., and S. R. Beissel. 1996. "Normalized smoothing functions for SPH impact computations." *International Journal for Numerical Methods in Engineering* 39 (16): 2725–2741.

Li, Z., J. Leduc, J. Nunez-Ramirez, A. Combescure, and J. C. Marongiu. 2015. "A non-intrusive partitioned approach to couple smoothed particle hydrodynamics and finite element methods for transient fluid-structure interaction problems with large interface motion." *Computational Mechanics* 55 (4): 697–718.

Liao, K., and C. Hu. 2013. "A coupled FDM-FEM method for free surface flow interaction with thin elastic plate." *Journal of Marine Science and Technology* 18 (1): 1–11.

Libersky, L. D., A. G. Petschek, T. C. Carney, J. R. Hipp, and F. A. Allahdadi. 1993. "High strain Lagrangian hydrodynamics." *Journal of Computational Physics* 109 (1): 67–75.

Lin, J., H. Naceur, D. Coutellier, and A. Laksimi. 2014. "Geometrically nonlinear analysis of thin-walled structures using efficient Shell-based SPH method." *Computational Materials Science* 85: 127–133.

Lin, J., H. Naceur, D. Coutellier, and A. Laksimi. 2015. "Geometrically nonlinear analysis of two-dimensional structures using an improved smoothed particle hydrodynamics method." *Engineering Computations* 32 (3): 779–805.

Lu, C. H., Y. S. He, and G. X. Wu. 2000. "Coupled analysis of nonlinear interaction between fluid and structure during impact." *Journal of Fluids and Structures* 14 (1): 127–146.

Lucy, L. B. 1977. "A numerical approach to the testing of the fission hypothesis." *The Astronomical Journal* 82: 1013–1024.

Marti, J., S. Idelsohn, A. Limache, N. Calvo, and J. D'Elia. 2006. "A fully coupled particle method for quasi-incompressible fluid-hypoelastic structure interactions." *Mecanica Computacional* 25: 809–827.

Maurel, B., and A. Combescure. 2008. "An SPH shell formulation for plasticity and fracture analysis in explicit dynamics." *International Journal for Numerical Methods in Engineering* 76 (7): 949–971.

Monaghan, J. J. 1994. "Simulating free-surface flows with SPH." *Journal of Computational Physics* 110 (2): 399–406.

Monaghan, J. J. 2005. "Smoothed particle hydrodynamics." *Reports on Progress in Physics* 68 (8): 1703–1759.

Monaghan, J. J., and R. A. Gingold. 1983. "Shock simulation by the particle method SPH." *Journal of Computational Physics* 52 (2): 374–389.

Morris, J. P. 1996. "Analysis of smoothed particle hydrodynamics with applications." Ph.D. thesis. Monash University.

Oger, G., M. Doring, B. Alessandrini, and P. Ferrant. 2006. "Two-dimensional SPH simulations of wedge water entries." *Journal of Computational Physics* 213 (2): 803–822.

Panciroli, R., S. Abrate, and G. Minak. 2013. "Dynamic response of flexible wedges entering the water." *Composite Structures* 99: 163–171.

Panciroli, R., S. Abrate, G. Minak, and A. Zucchelli. 2012. "Hydroelasticity in water-entry problems: Comparison between experimental and SPH results." *Composite Structures* 94 (2): 532–539.

Panciroli, R., and M. Porfiri. 2015. "Analysis of hydroelastic slamming through particle image velocimetry." *Journal of Sound and Vibration* 347: 63–78.

Potapov, S., B. Maurel, A. Combescure, and J. Fabis. 2009. "Modeling accidental-type fluid-structure interaction problems with the SPH method." *Computers & Structures* 87 (11-12): 721–734.

Rafiee, A., and K. P. Thiagarajan. 2009. "An SPH projection method for simulating fluid-hypoelastic structure interaction." *Computer Methods in Applied Mechanics and Engineering* 198 (33-36): 2785–2795.

Shao, S. 2009. "Incompressible SPH simulation of water entry of a free-falling object." *International Journal for Numerical Methods in Fluids* 59 (1): 91–115.

Skillen, A., S. Lind, P. K. Stansby, and B. D. Rogers. 2013. "Incompressible smoothed particle hydrodynamics (SPH) with reduced temporal noise and generalised Fickian smoothing applied to body-water slam and efficient wave-body interaction." *Computer Methods in Applied Mechanics and Engineering* 265: 163–173.

Stenius, I., A. Rosen, M. Battley, and T. Allen. 2013. "Experimental hydroelastic characterization of slamming loaded marine panels." *Ocean Engineering* 74: 1–15.

Sun, P., F. Ming, and A. Zhang. 2015. "Numerical simulation of interactions between free surface and rigid body using a robust SPH method." *Ocean Engineering* 98: 32–49.

Swegle, J. W. 2000. *Conservation of momentum and tensile instability in particle methods.* Tech. rep.. Sandia National Labs.

Swegle, J. W., D. L. Hicks, and S. W. Attaway. 1995. "Smoothed particle hydrodynamics stability analysis." *Journal of Computational Physics* 116 (1): 123–134.

Tofighi, N., M. Ozbulut, A. Rahmat, J. J. Feng, and M. Yildiz. 2015. "An incompressible smoothed particle hydrodynamics method for the motion of rigid bodies in fluids." *Journal of Computational Physics* 297: 207–220.

Vidal, Y., J. Bonet, and A. Huerta. 2007. "Stabilized updated Lagrangian corrected SPH for explicit dynamic problems." *International Journal for Numerical Methods in Engineering* 69 (13): 2687–2710.

Walhorn, E., A. Kolke, B. Hubner, and D. Dinkler. 2005. "Fluid-structure coupling within a monolithic model involving free surface flows." *Computers & Structures* 83 (25-26): 2100–2111.

Wang, X., X. Gu, P. Temarel, and J. Hu. 2016. "Investigation of springing in ship structures using experimental methods and 3-D hydroelastic theory." *Journal of Marine Science and Technology* 21 (2): 271–281.

Yang, Q., V. Jones, and L. McCue. 2012. "Free-surface flow interactions with deformable structures using an SPH-FEM model." *Ocean Engineering* 55: 136–147.